Random lasing in closely packed resonant scatterers

Xiaohua H. Wu, Alexey Yamilov, Heeso Noh, and Hui Cao

Department of Physics and Astronomy, Materials Research Center, Northwestern University, Evanston, Illinois 60208

Eric W. Seelig and Robert P. H. Chang

Department of Materials Science and Engineering, Materials Research Center, Northwestern University, Evanston, Illinois 60208

Received April 15, 2003; revised manuscript received July 24, 2003; accepted August 4, 2003

We report experimental and theoretical studies of the random lasing threshold and its fluctuation in an ensemble of highly packed spherical dielectric scatterers. The ratio of the sphere diameter to the lasing wavelength was varied in a wide range, which covered the transition from the weak Rayleigh scattering regime to the strong Mie scattering regime. Experimentally, when the diameters of monodispersed ZnO spherical particles changed from less than 100 to more than 600 nm we observed a drastic decrease of the lasing threshold at small-particle size followed by a plateau at large particle size. We attribute this effect to the particle-size dependence of transport mean free path l_t, which was deduced from coherent backscattering measurements. Theoretical calculation of l_t reproduced experimental behavior. Using the finite-difference time domain method, we obtained the lasing threshold and its standard deviation as functions of particle size in two-dimensional systems. The results of our numerical simulations are in qualitative agreement with the experimental data.

OCIS codes: 290.4210, 140.3460.

1. INTRODUCTION

The random laser is a special kind of laser whose feedback is due to light scattering instead of to reflection. After the pioneering research of Letokhov in 1968,[1] the study of the random laser was renewed in the past decade with the experimental demonstration of an incoherent random laser and a coherent random laser.[2] The active random media used for the random laser can be divided into two categories: passive scatterers doped in a gain medium, e.g., titanium dioxide microparticles in a dye solution, and aggregations of active scatterers such as ZnO powder. In the former, gain media and scattering centers are separated; thus the amount of gain and the amount of scattering can be varied independently. However, the scattering strength of the latter is usually higher than of the former, owing to a larger contrast of refractive index and a higher density of scatterers. Hence the lasing threshold is lower in the second type of random medium. Nevertheless, the threshold of a random laser is still too high for practical applications. Further reduction of the lasing threshold requires better confinement of light in the random medium through stronger scattering. It is well known that light scattering by dielectric particles is strongly enhanced at Mie resonances. Recently Chabanov and Genack observed photon localization in resonant media at the frequency near the first Mie resonance.[3] That research inspired us to use closely packed resonant scatterers for a random laser. We synthesized monodisperse ZnO nanospheres and closely packed them at high pressure. The mean diameter of ZnO spheres varied over a wide range and covered several Mie resonances for the ZnO emission wavelength. Apalkov *et al.* showed that the likelihood of finding a random resonator of high quality increases dramatically with increasing correlation radius.[4] A drastic increase in the correlation radius near Mie resonance would lead to the formation of high-Q cavities and to the reduction of the lasing threshold. We measured the random lasing threshold in closely packed ZnO powder. When the diameter of monodispersed ZnO spherical particles changed from less than 100 to more than 600 nm, we observed a drastic decrease in the lasing threshold at small-particle size, followed by a plateau at large-particle size. This dependence was attributed to a change of scattering strength in our samples.

In a scattering medium there are two characteristic length scales that determine light transport properties. When a coherent pulse of electromagnetic radiation is incident on a system containing scattering centers, the energy of the beam is exponentially attenuated with scattering length l_{sc}. Theoretically, l_{sc} is usually determined from the average (field) Green function, where the effect of scattering is manifested as a complex part of the refractive index of the effective medium. What appears to be a loss for coherent beam is, in fact, converted into multiply scattered waves that propagate diffusely.[5,6] For sufficiently thick systems the energy transport is dominated by diffusion because of a much slower power-law dependence on sample thickness. Transport length l_t that governs the diffusive energy transfer enters the diffusive equation for averaged intensity; it is, therefore, a property of the averaged product of two Green functions or, al-

ternatively, of the correlation function. It is worthwhile mentioning that the wave nature of light is ignored in the regular diffusion equation. Wave interference effects result in the corrections that lead to interesting phenomena, of which coherent backscattering (CBS) is, probably, the most prominent.[7,8] In our experiment we utilized CBS to extract the value of l_t. Theoretically we propose to determine l_t from the exact solution[9] of the scattering problem for the clusters of dielectric spheres. This calculation allows us to find l_t in the regime of strong scattering.

In a random laser, not only the mean value of the lasing threshold but also its fluctuation is an important characteristic of the system. Unlike that of a conventional laser, the random laser's threshold varies from sample to sample. Such variation is intrinsic; i.e., samples with the same scattering length may have different lasing thresholds. The variation of lasing threshold reflects the statistical distribution of a random cavity-quality factor. Patra calculated the distribution of lasing threshold in both diffusion and localization regimes.[10] Although threshold variation is an important characteristic of a random laser, there has been no experimental measurement of it so far, to our knowledge. In a previous experiment with polydisperse powder we measured the lasing threshold in different parts of the same sample. The sample's nonuniformity led to fluctuation of the scattering length across the powder, and it added an artificial variation to the intrinsic variation of random lasing threshold. Using monodisperse ZnO spheres, we were able to make uniform random samples. In this paper we report our measurement and numerical simulation of the fluctuation of lasing threshold in samples of different scattering lengths.

Theoretically, finding the threshold of a random laser is a difficult problem. The states responsible for the lasing threshold are those with the smallest leakage. Therefore they should contribute least to the transport properties that have been extensively studied. The finite-difference time-domain method[11] has turned out to be a reliable tool in the investigation of the random laser in one dimension[12] and two dimensions.[13] Here we report the finite-difference time-domain–based calculation of the lasing threshold in random media of monodisperse scatterers, where we have obtained good qualitative agreement with the experiment. At present, our numerical simulation of sufficiently large systems is possible only in two dimensions.

2. EXPERIMENTS

The ZnO particles were synthesized in a two-stage reaction process. Experimental apparatus and fabrication procedures were described previously.[14] In a typical reaction, 0.03 mol. of ZnAc was added to 300 mL of diethylene glycol and heated under reflux to 160 °C. Shortly after the solution reached that temperature, precipitation of ZnO occurred. After the product solution was centrifuged, the supernatant (diethylene glycol, dissolved reaction products, unreacted ZnAc, and water) was decanted and saved. The polydisperse ZnO particles were discarded. A secondary reaction was then produced as described above, except that before precipitation (typically at 150 °C) some amount of the supernatant of the primary reaction was added to the solution. Following the addition there was a temperature drop, and precipitation occured at a temperature lower than 160 °C. We washed and dried the precipitant to get a white, fine ZnO powder. A scanning-electron microscope (SEM) image showed that the powder consisted of monodisperse spheres. The dispersion of the spheres diameter was 5–8%. By adding different amounts of supernatant before precipitation, we varied the mean diameter of ZnO spheres from 85 to 617 nm. High-resolution SEM images revealed that individual spheres consist of many ZnO nanocrystallites. X-ray diffraction data showed that the sizes of these nanocrystallites were 10–15 nm for all the ZnO spheres of different diameters.

We cold-pressed ZnO spheres with a pressure of 150 MPa to form pellets of diameter 7.9 mm and thickness 1.4 mm. Because we used the same amount (0.17 g) of powder and made pellets of the same volume, the densities ρ of all the pellets made from different-diameter spheres were the same. Thus the ZnO filling factors of all the pellets were the same: $f = \rho/\rho_0 \sim 45\%$, where ρ_0 is the density of ZnO crystals. Figure 1 shows SEM images (top view) of two pellets made from ZnO spheres with mean diameters of 85 and 617 nm. Because ZnO spheres are porous and are composed of nanocrystallites, the ef-

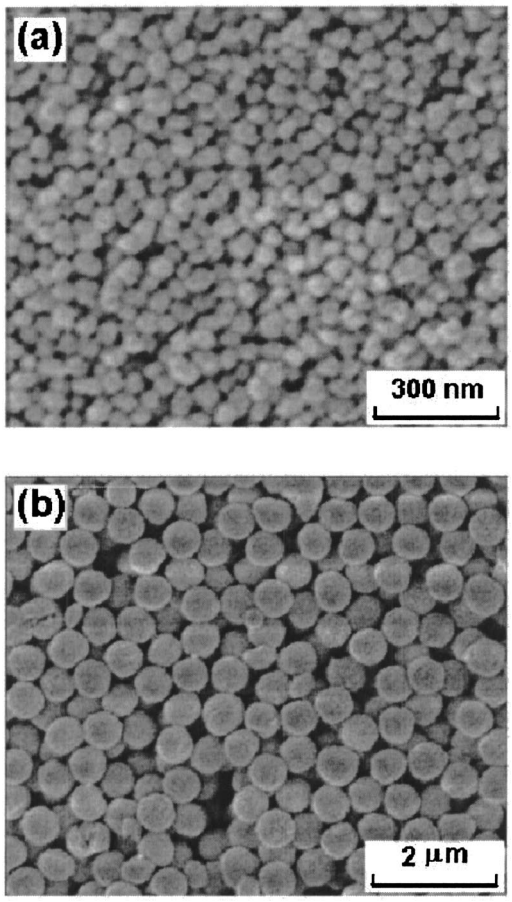

Fig. 1. SEM images (top view) of two pellets made from ZnO spheres with mean diameters (a) $d = 85$ nm and (b) $d = 617$ nm.

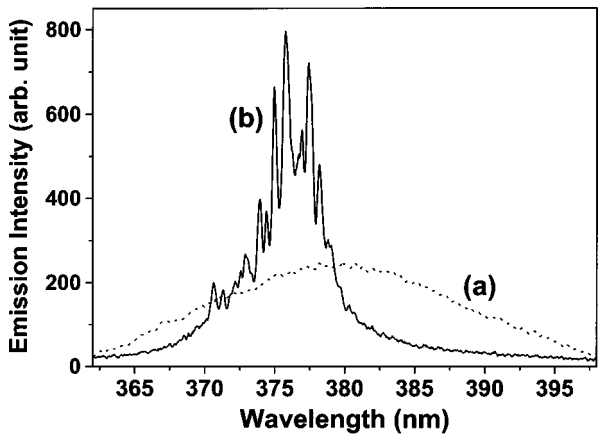

Fig. 2. Measured spectra of emission from a ZnO pellet. The mean diameter of the ZnO spheres is 617 nm. The pump beam spot on the sample surface is 8 μm in diameter. The incident pumping intensities are (a) 6 MW/mm^2 and (b) 11 MW/mm^2. The integration times are (a) 15 and (b) 3 s.

fective index of refraction n for ZnO spheres is lower than that of ZnO crystals. In previous research, the present authors and others[14] arranged the ZnO spheres in a fcc structure and measured the transmission spectrum. The dip in the transmission spectrum gave the frequency of the photonic band gap in the (111) direction. From it, we inferred the effective index of refraction $n \sim 1.7$; the volume fraction of ZnO nanocrystallites inside a single sphere was ~77%. Therefore the volume fraction of the ZnO spheres in the pellet was ~58%. This number confirms that ZnO spheres are closely packed. Unlike sedimentation, our process of packing ZnO spheres was so fast that the spheres had no time to arrange themselves into ordered structures. Hence the ZnO spheres were randomly positioned, as can be seen from the SEM images.

In the lasing experiment the samples were optically excited by the third harmonic of a mode-locked Nd:YAG laser ($\lambda = 355$ nm, 10-Hz repetition rate, 20-ps pulse width). The pump beam was focused to a spot on the sample's surface at normal incidence. The emission spectra were measured by a spectrometer with 0.13-nm spectral resolution. As shown in Fig. 2, at low excitation intensity the spectrum had a single, broad spontaneous-emission peak. As the pump intensity increased, the emission peak was gradually narrowed as a result of amplified spontaneous emission. When the excitation intensity exceeded a threshold, extremely narrow peaks emerged near 375 nm. With a further increase of the pump intensity, more sharp peaks appeared. Figure 3 is a plot of the lasing threshold pump intensity versus the ZnO sphere diameter for two pump areas. When the diameter of the excitation spot was changed from 8 to 16 μm, the lasing threshold exhibited a similar dependence on sphere size. There are two distinct features in Fig. 3: first, the threshold pump intensity remains nearly constant for a wide range of sphere diameters from 137 to 617 nm; second, with a small decrease of sphere diameter from 137 to 114 nm, the lasing threshold increases dramatically, especially for smaller pump area. For the sample of 85 nm spheres, we could observe only amplified spontaneous emission but not lasing. The lasing threshold pump intensity for a larger pump area was lower than that for a smaller pump area, consistent with our previous finding.[15]

Previously we had seen that the size of random laser cavities decreases with transport mean free path l_t.[16] Better confinement also results in higher cavity Q and, therefore, in lower threshold. To test this hypothesis, first we determined how the scattering strength of an individual sphere changes with the sphere's size. The inset of Fig. 3 shows the ratio of the scattering cross section to the geometric cross section relative to sphere diameter d at a lasing wavelength of 375 nm. In the calculation we used the effective refractive index $n = 1.7$ for the ZnO spheres. The dotted lines indicate the range of the diameters of ZnO spheres that we fabricated. Thus the range of monodisperse ZnO sphere sizes in our random lasing experiment covered the first few Mie resonances at the ZnO emission wavelength. The Mie resonances were broad owing to the relatively low refractive index of ZnO spheres. Scattering cross section σ_{sc} exhibited a drastic increase with sphere diameter d before reaching the first Mie resonance. In such densely packed systems as ours, the scattering strength of a single particle can be significantly modified by the interactions. The CBS experiment allowed us to measure the dependence of the transport mean free path l_t on the sphere diameter directly.

In our CBS measurements the angular resolution was 0.01°. l_t was measured at three wavelengths with three laser sources: a cw He–Ne laser ($\lambda = 633$ nm), a mode-locked Ti:sapphire laser ($\lambda = 792$ nm), and the second harmonics of the Ti:sapphire laser ($\lambda = 400$ nm). All the probe beams were well collimated to a spot of 4-mm-diameter on the pellet surface. To obtain a speckle-free CBS cone we, rotated the pellet at ~100 rpm about an axis normal to the pellet's flat surface. Figure 4 shows the CBS cones of a ZnO pellet ($d = 233$ nm) at three wavelengths. We derived the transport mean free path l_l from the full width at half-maximum of a CBS cone after taking the surface reflection into account.[17]

Figure 5 shows transport mean free path l_t versus ZnO particle diameter d at three wavelengths. First we can

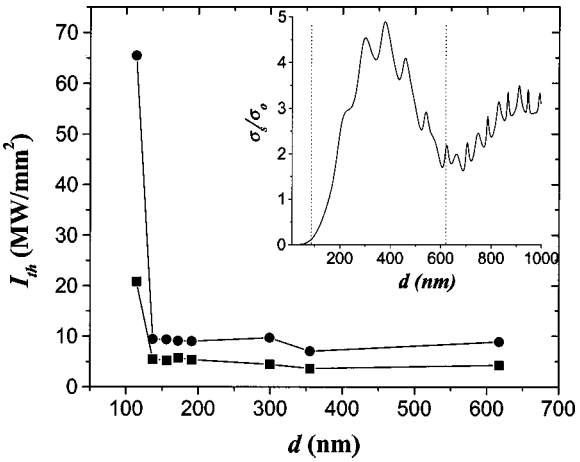

Fig. 3. Measured incident pump intensity at lasing threshold I_{th} versus ZnO sphere diameter d. Circles and squares correspond to pump spot diameters of 8 and 16 μm, respectively. Inset, calculated normalized scattering cross section σ_{sc}/σ_g of a single ZnO sphere as a function of its diameter d.

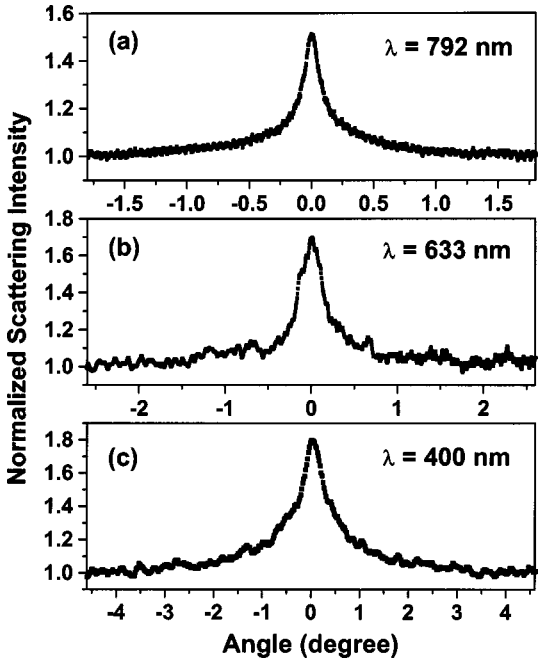

Fig. 4. Measured CBS cones of the same ZnO pellet at three wavelengths λ. The mean diameter of the ZnO spheres is 233 nm.

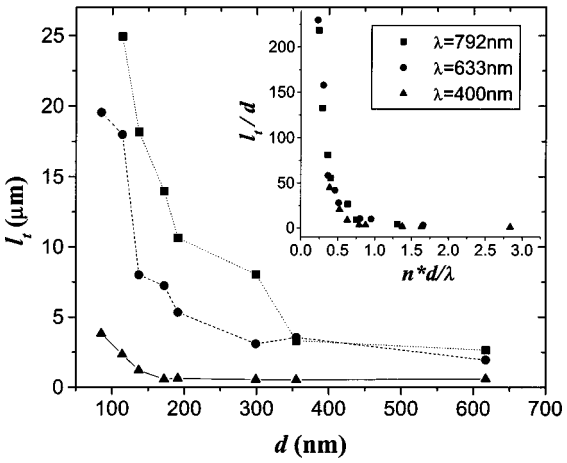

Fig. 5. Measured transport mean free path l_t versus ZnO sphere diameter d at wavelengths λ = 400, 633, 792 nm. Inset, measured l_t/d versus nd/λ.

see that, for all three λ, the transport mean free path l_t varied as d varied. When d increased, l_t first decreased rapidly and then saturated. For λ = 400 nm, l_t decreased from 4.4 μm at d = 85 nm to 0.6 μm at d = 172 nm. l_t was more than seven times shorter for only an 87-nm change of the sphere diameter. For λ = 633 nm, l_t decreased from 19.5 μm at 85 nm to 3.1 μm at 299 nm; it was more than six times shorter for an ~200 nm change in d. For λ = 792 nm, l_t decreased from 25 μm at 114 nm to 3.3 μm at 355 nm, approximately eight times shorter after a 240-nm change. So the decrease was most abrupt for λ = 400 nm. However, after l_t/d of all three measurements was plotted versus the dimensionless parameter $y = nd/\lambda$ (inset of Fig. 5), the dependence of l_t/d on y became universal. In Section 3 below we shall see that the crossover from rapid decrease to saturation can be explained by the transition from the Rayleigh[18] weak-scattering regime to the Mie strong-scattering regime, which is governed by the parameter y. This transport mean-free-path measurement confirms our hypothesis about the direct relation between l_t and the value of the lasing threshold.

The lasing threshold varied as we excited different parts of the same sample. In fact, the lasing thresholds shown in Fig. 3 are the mean values of threshold pump intensities. The statistical fluctuation of the lasing threshold is an important property of a random laser. To fully understand the random laser's behavior, we measured the variance of the lasing threshold pump intensities. Experimentally, we shifted the pump spot across the sample and recorded the lasing threshold pump intensity I_{th}. The diameter of the excitation spot was kept constant. Then we calculated the mean value $\langle I_{\mathrm{th}}\rangle$ and its standard deviation $\mathrm{std}(I_{\mathrm{th}}) = [\langle(I_{\mathrm{th}} - \langle I_{\mathrm{th}}\rangle)^2\rangle]^{1/2}$. The normalized standard deviation was $\delta\gamma/\langle\gamma\rangle = \mathrm{std}(I_{\mathrm{th}})/\langle I_{\mathrm{th}}\rangle$. We found experimentally that the variance for 400 threshold data has the same value as that for 200 data. Therefore we used 200 threshold data to get the variance of the lasing threshold. Table 1 lists some of our experimental results. The standard deviation of the lasing threshold decreased with increasing sphere diameter d. However, for the largest d the standard deviation increased slightly. As discussed above, in the pellets composed of larger ZnO spheres, shorter l_t resulted in smaller lasing cavities.

Within a constant pump area there are more random laser cavities available. The improved averaging within the pump area leads to smaller fluctuation of the lasing threshold. This explains the decrease in the deviation of the lasing threshold with increasing sphere diameter d. Typically there are many spheres within the pumped region. Although the particle configurations change with the pump positions, different pump regions of the same sample are statistically equivalent. However, when the ZnO spheres are as large as 617 nm, the number of spheres within the pumped region is rather small. At different pump positions, the number of spheres and their configuration can be quite different. This may cause more fluctuation in lasing threshold. To test the above explanation we increased the pump area to 15 μm in diameter and measured the variance of lasing threshold for two samples (d = 137 nm and d = 299 nm). The normalized deviation for the d = 137 nm sample was $\delta\gamma/\langle\gamma\rangle$ = 11%. It was larger than the 7% deviation of the d = 299 nm sample that had shorter l_t. We also compared the fluctuation of the lasing threshold for the

Table 1. Fluctuation of Lasing Threshold in Five Samples with 5-μm Pump Area

Sample Number	d (nm)	l_t (μm)	$\langle I_{\mathrm{th}}\rangle$ (MW/mm^2)	std(I_{th}) (MW/mm^2)	$\delta\gamma/\langle\gamma\rangle$ (%)
1	137	1.21	20.8	3.5	17
2	172	0.58	19.1	2.0	11
3	299	0.55	19.6	1.5	8
4	355	0.53	16.8	1.2	7
5	617	0.61	17.4	1.7	10

same sample at different pump diameters s. For $d = = 137\,\mathrm{nm}$, $\delta\gamma/\langle\gamma\rangle = 17\%$ at $s = 5\,\mu\mathrm{m}$, larger than $\delta\gamma/\langle\gamma\rangle = 11\%$ at $s = 15\,\mu\mathrm{m}$. In the smaller pumped region, fewer random laser cavities are available, leading to larger threshold fluctuation. For $d = 299\,\mathrm{nm}$ the two deviations were similar, $\delta\gamma/\langle\gamma\rangle = 8\%$ at $s = 5\,\mu\mathrm{m}$ and $\delta\gamma/\langle\gamma\rangle = 7\%$ for $15\,\mu\mathrm{m}$. This may be due to the accuracy of our threshold measurement. Because of power fluctuation of our pump laser, we could not resolve the small difference in threshold fluctuation.

3. THEORY

For a quantitative understanding of our experimental results, we calculated the transport mean free path as well as the scattering mean free path. We also simulated the lasing threshold for both TE and TM polarization in two-dimensional (2D) random systems.

A. Transport Length in a Closely Packed System of Monodisperse Spheres

Calculation of the scattering length is relatively easier than calculation of l_t. If scattering is weak, i.e., if $kl_{\mathrm{sc}} \gg 1$, frequency dispersion becomes simple (the on-shell approximation is valid), which allows for a simple solution[6]:

$$l_{\mathrm{sc}}(\omega) = \frac{1}{\rho\sigma_{\mathrm{sc}}(\omega)}, \tag{1}$$

where ρ is the density of scatterers and $\sigma_{\mathrm{sc}}(\omega)$ is frequency-dependent scattering strength (cross section) of an individual particle. Here, only the scattering characteristics of a single scattering center enter into the expression for l_{sc}. This is certainly an approximation that is satisfied well in the weak-scattering limit. Indeed, when scattering becomes stronger, light propagation can no longer be regarded as a sequence of scattering events from one particle at a time: Dependent scattering becomes important. When interaction between scatterers is insignificant, one can find a connection between l_{sc} and l_t—our quantity of interest:

$$l_t(\omega) = \frac{l_{\mathrm{sc}}(\omega)}{1 - \langle\cos\theta(\omega)\rangle}, \tag{2}$$

where θ is the scattering angle and $\langle\ \rangle$ signifies an angular average weighted by the differential cross section. The denominator of Eq. (2) accounts for angular dependence of the scattering cross section. For a coherent beam (l_{sc}) the scattering angle is of no importance: Once scattering occurs, the photon is removed from the beam, regardless of the new direction. The scattering direction can be close to the original direction of propagation, which would affect how the energy is transferred diffusely. The presence of $\langle\cos\theta(\omega)\rangle$ accounts for the change in direction of propagation.

In a closely packed mixture of spherical scatterers the regime of weak, independent scattering can still be satisfied when particles are small compared to the wavelength of light, i.e., the Rayleigh limit, $x = 2\pi r/\lambda \ll 1$. Here x is the so-called size parameter related to parameter nd/λ that we use in this paper, and r is the particle radius. Scattering is dominated by dipole scattering, where the cross section can be written in the leading order in x as[18]

$$\sigma_{\mathrm{sc}} = \frac{8}{3}x^4\left(\frac{n^2 - 1}{n^2 + 2}\right)^2\sigma_g, \tag{3}$$

where σ_g is the geometrical cross section πr^2. Small x expansion of $\langle\cos\theta(\omega)\rangle$ starts with a quadratic term and, therefore, would lead to higher-order correction in Eq. (2). In our system the scattering cross section is not the only source of particle-size dependence of l_t. Indeed, when the particle size was reduced under constant filling fraction f, density ρ changed as $\rho = f/(4\pi r^3/3)$. Finally, in the Rayleigh limit we obtained

$$l_{\mathrm{sc}} \simeq l_t \simeq \frac{\lambda}{4f\pi^4}\left(\frac{\lambda}{d}\right)^3\left(\frac{n^2 + 2}{n^2 - 1}\right)^2. \tag{4}$$

Strong third-power dependence on the particle diameter resulted in a sharp decrease in the transport length seen in the experiment (Fig. 5). This approximation broke down at[18] $x \simeq 0.8$ or, in terms of particle size, $d \simeq 100\,\mathrm{nm}$, which corresponds to the transition to the strong scattering regime to be discussed below. The predicted crossover size was in good agreement with the experiment.

For larger sizes, individual sphere scattering becomes so strong that the interaction between scatterers cannot be ignored. This means that σ_{sc} can no longer be described by Eq. (3). One of the straightforward approaches to improving Eqs. (1) and (2) in this regime is to calculate the second-order correction in density. This turns out to be a difficult task; exact calculations could be performed for a Gaussian fluctuation model of correlated disorder.[19] This model, well suited for the porous silica sample of Ref. 19, may not give all the structure that resulted from the sample of monodisperse spheres considered in this paper.

Another highly accurate approximation that is widely used for calculating l_{sc} is the coherent potential approximation (CPA).[6,20,21] Within the CPA one calculates the effective dielectric constant (its imaginary part is related to l_{sc}) of the medium, taking into consideration the microstructure of the system. For monodisperse spheres, one considers a single sphere surrounded by an air shell, embedded in the effective medium. Self-consistency requires the disappearance of scattering in the forward direction. Extensions of CPA allow for more-complex scattering units as well as for the correction that is due to modified dispersion,[21] which becomes important[22] in strong-scattering cases.

To determine the transport mean free path, Busch *et al.*[23] proposed to calculate $\sigma_t = \int \mathrm{d}\Omega\,\sigma_{\mathrm{sc}}(\Omega)[1 - \cos(\theta)]$ for the CPA unit, where the integral of the solid angle is taken. Comparing this expression with Eqs. (1) and (2), one can see that this is an extension of the weak-scattering formula into the strong-scattering regime, replacing the real single scatterer by an effective scatterer.

In the strong-scattering regime CPA calculations with needed corrections[20,21,23,24] become increasingly complicated and computationally heavy. In the remainder of this section we present a relatively easy way to calculate

l_{sc} and l_t for a monodisperse ensemble of dielectric spheres with large size parameter $x = kr$.

The solution of the scattering problem of a single dielectric sphere, the Mie solution, is well known.[18,25] Recently it was proposed to use truncated multipole expansions to solve the multisphere problem (see Ref. 9 and references therein). Within this generalized multisphere Mie solution one expands the electric field inside and outside each sphere in vector spherical harmonics; then the field incident upon a sphere is the sum of the incoming plane wave and fields scattered by all other spheres. By matching the boundary conditions on the sphere surfaces one obtains a linear system on the spherical harmonic coefficients, which is solved by recursion.[9] To obtain scattering coefficients one adds the individual scattered fields in the far-field zone. The computation time depends strongly on size parameter x, as the number of multipoles needed for convergence increases with x. We note from the SEM images that the ZnO particles, apart from size dispersion, are not perfect spheres. In our calculation the shape of the particles is assumed to be exactly spherical. This is a usual assumption in all theoretical models that include CPA. Like size dispersion, shape deformation of ZnO particles will smooth out any sharp resonance features found in the modeling. However, lack of sharp resonances in the regime of relatively small size parameter x will diminish the effect of shape deformation.

Like Busch *et al.*[23] and Busch and Soukoulis,[24] we define l_{sc} and l_t in the strongly scattering regime as in Eqs. (1) and (2), but instead of basing our calculations of $\sigma_{sc}(\omega)$ and $\langle\cos(\theta)\rangle$ on the CPA we calculate these quantities for the individual spheres inside the finite clusters. More precisely, we (i) generate 10 clusters, each of 5 or 10 randomly arranged dielectric spheres with filling fraction $f \simeq 0.5$; (ii) solve the scattering problem, using the generalized multisphere Mie code; (iii) find $\sigma_{sc,i}(\omega)$ and $\langle\cos(\theta_i)\rangle$ for each sphere in the cluster, averaged over 24 angular orientations of the cluster and 2 polarizations of the incident field; and (iv) compute average $\sigma_{sc}(\omega)$ and $\langle\cos(\theta)\rangle$ over all spheres in the cluster and in the 10 random configurations. To match our experimental setup we chose spheres with refractive index $n = 1.7$ and $nd/\lambda \in [0, 4]$.

It is illuminating to note that σ_t, defined in Ref. 23, in a lossless system is a called radiative pressure cross section, σ_{pr}.[18,26] In the more general case of absorbing particles,

$$\sigma_{pr} = \sigma_{ext} - \sigma_{sc}\langle\cos(\theta)\rangle = \sigma_{abs} + \sigma_{sc}[1 - \langle\cos(\theta)\rangle], \tag{5}$$

where σ_{ext} and σ_{abs} are extinction and absorption cross sections, respectively. Equation (5), after multiplication by density ρ, leads to the well-known[27] diffusion formula $l^{-1} = {l_{abs}}^{-1} + {l_t}^{-1}$. This fact allows us to extend our approach to absorbing media as well; absorbing media are not addressed further in the present paper. We should also stress that our calculations become incorrect when l_{sc} becomes larger than the size of the cluster, which restricts us to $y = nd/\lambda > 1$. This is, however, the region where the weak-scattering approximation described at the beginning of this section gives reliable results. Therefore the combination of the weak-scattering approximation with the cluster-based calculation gives continuous coverage for practically all values of y.

The results of the calculations outlined above are presented in Figs. 6 and 7. The inset of Fig. 6 shows a significant modification of the scattering efficiency of the particles in the cluster as a result of interaction among particles. When the resonant scatterers with scattering cross sections larger than their geometrical cross sections are packed closely together, hybridization caused by interaction (dependent scattering) occurs. As a result, $\langle\sigma_{sc}\rangle/\sigma_g$ saturates at $\sim f^{-2/3}$, the square of the average

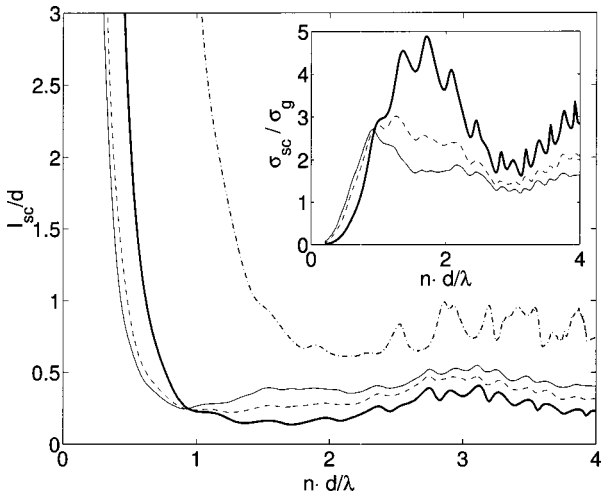

Fig. 6. Calculated scattering length l_{sc} normalized by sphere diameter d calculated for clusters of 5 (dashed curve) and 10 (solid thinner curve) spheres as a function of normalized particle size nd/λ. The solid thicker curve represents l_{sc} calculated within an independent scattering approximation. The dashed–dotted curve gives the energy-density CPA result[24] for $f = 0.5$, $n = 1.7$. Inset, calculated scattering efficiencies σ_{sc}/σ_g of a stand-alone single sphere (darker solid curve) and of spheres in clusters of 5 (dashed curve) and 10 (lighter solid curve) particles.

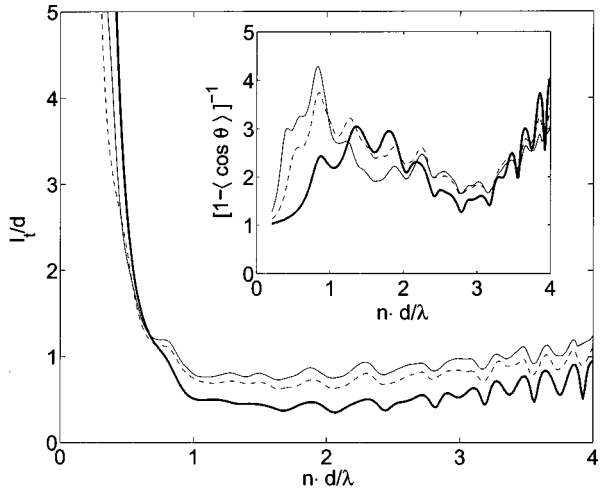

Fig. 7. Calculated transport mean free path l_t normalized by sphere diameter d calculated for clusters of 5 (dashed curve) and 10 (thinner solid curve) spheres as a function of normalized particle size nd/λ. The thicker solid curve represents l_t calculated within an independent scattering approximation. Inset, calculated value of $\langle\cos(\theta)\rangle$ of a stand-alone single sphere (thicker solid curve), and spheres in clusters of 5 (dashed curve) and 10 (thinner solid curve) particles.

(dimensionless) distance between scatterers. When such saturation occurs, $l_{sc}^{-1} \simeq \rho f^{-2/3}\sigma_g \propto (df^{-1/3})^{-1}$. Normalized by the particle size, l_{sc}/d appears to be a constant, as can be seen from Fig. 6. The residual structure can be traced back to the single-particle resonances and would probably not survive a small-sized dispersion, which would be inevitable in the experiment. In Fig. 6 we have also plotted the scattering length calculated with the energy-density CPA method[24] (dashed–dotted curve). For the CPA calculation we used the same parameters as for the calculation by the cluster method: $\lambda = 375\,\text{nm}$, $d = [0\,\text{nm}, 900\,\text{nm}]$, $n = 1.7$, and filling fraction $f = 0.5$. In the region of applicability of the cluster method ($nd/\lambda > 1$) we observed that the values of l_{sc} obtained with the cluster method are ~30% smaller than those given by the CPA. This discrepancy may be partially due to the finite size of the cluster.

In the inset of Fig. 7 we have plotted $[1 - \langle\cos(\theta)\rangle]^{-1}$ for a particle in a cluster. The first obvious characteristic is that the scattering within the cluster is highly anisotropic. This anisotropy may be attributed to the fact that many scatterers lie close to boundary and may not sense the local environment as well as those inside the cluster. We did not, however, notice any systematic difference in $\langle\cos(\theta)\rangle$ for these two types of particle. Another important consequence of combining l_{sc} and $\langle\cos(\theta)\rangle$ in Eq. (1) is the disappearance of most of the irregular structure inherited from l_{sc}. Indeed, l_t is a strikingly smoother function of the particle size, which reproduces well the experimentally observed situation reported in Section 2. The similarity between l_t calculated for clusters of 5 and 10 spheres and the fact that l_t is smaller than the cluster size demonstrate that we have captured the most important effects of dependent scattering. Even though extending the calculations to larger clusters would improve our results, it would not change them significantly. The absence of systematic differences in scattering properties among the particles in the cluster further confirms this conclusion.

B. Numerical Simulation of the Laser Threshold and Its Fluctuations

To find the lasing threshold we assume that it is determined solely by the mode of the lowest radiative loss, the highest quality factor Q_m. This is a simplification that neglects nonuniformity of the gain in the system. We believe, however, that qualitative dependence should not be affected by this assumption. The system under consideration is a 2D array of passive dielectric rods with refractive index $n = 2.2$ and a filling fraction of 0.5. When we changed the size (diameter) of the rods, $nd/\lambda_0 \in [0.2, 2]$, we kept the physical size of the system constant at $2\,\mu\text{m} \times 2\,\mu\text{m}$ with wavelength $\lambda_0 = 375\,\text{nm}$. To determine the quality factor of the least leaky mode, we launched a pulse with a bandwidth of ~10 nm centered at λ_0. After initial excitation the modes in the excited frequency region decayed with time. After a sufficient time, only one mode, that with the highest Q, dominated the spectrum, as was evidenced by the stabilized field distribution in the sample. In this regime the total energy stored in the system followed a single exponential decay with time: $\mathcal{E} \propto \text{Re}[\exp 2i\omega_m(1 + i/2Q_m)t]$. From this dependence, frequency ω_m and quality factor Q_m were determined by use of a Fourier transform. As the lasing threshold is inversely proportional to the maximum Q, we define the lasing threshold in our system as $\gamma \equiv 1/Q_m$. For 100 examples of disorder we calculated the mean value of the lasing threshold $\langle\gamma\rangle$ and its standard deviation, $\delta\gamma$. To make a comparison with experiments done in three dimensions we performed calculations for both TM (E field parallel to the cylinder axis) and TE (H field parallel to the cylinder axis) polarization. It can be shown that Maxwell's equations for TM polarization are equivalent to scalar equations. For this reason, TM polarization is sometimes called s polarization, as opposed to p or TE polarization. For TE polarization, two components of the electric field are available, which makes the experiments more like three-dimensional experiments.

The squares in Figs. 8 and 9 show the results for TM polarization. One can see that there are three minima of lasing threshold, at $nd/\lambda = 0.6, 1, 1.4$. As the values of $\delta\gamma$ remain approximately the same (Fig. 9), they lead to sharp peaks of $\delta\gamma/\langle\gamma\rangle$. These peaks can be shown to be related to the bandgaps of the ordered sample with the same filling ratio. Preliminary results related to the bandgap of the spectrum were reported in Ref. 28, with a report of a more-detailed study planned, those early results are not discussed further in this paper. Apart from bandgap-related minima of $\langle\gamma\rangle$, and more relevant to the current discussion, the dependence of threshold on size is featureless. The threshold is almost constant, with no increase at the small-particle size, in contrast to the experimental result reported earlier in this paper and to the numerical calculation for TE polarization (Fig. 8). Indeed, TE polarization does show a drastic decrease of $\langle\gamma\rangle$ at $nd/\lambda \simeq 0.5$, which is similar to the characteristic size both in experiment and in the three-dimensional (3D) theoretical prediction for l_t. Naturally the question arises: Why does TM polarization show such a remarkable difference from TE polarization?

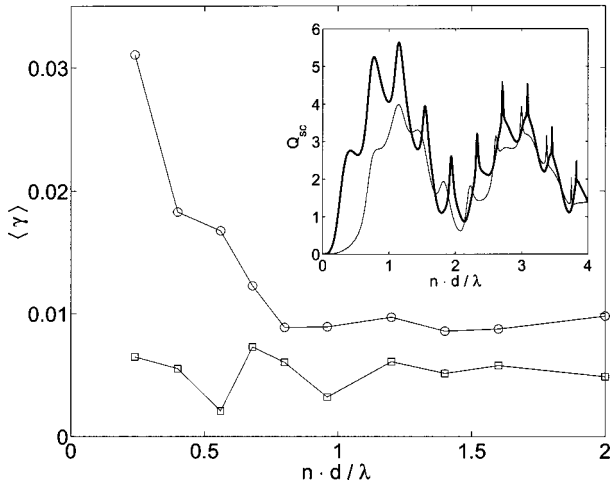

Fig. 8. Calculated average lasing threshold $\langle\gamma\rangle = \langle 1/Q\rangle$ as a function of dimensionless particle size. Squares and circles represent TM and TE polarization, respectively. Error bars are too small to be shown. Inset, calculated scattering efficiency of a dielectric cylinder with $n = 2.2$ for TE (thinner curve) and TM (thicker curve) polarization versus the dimensionless diameter.

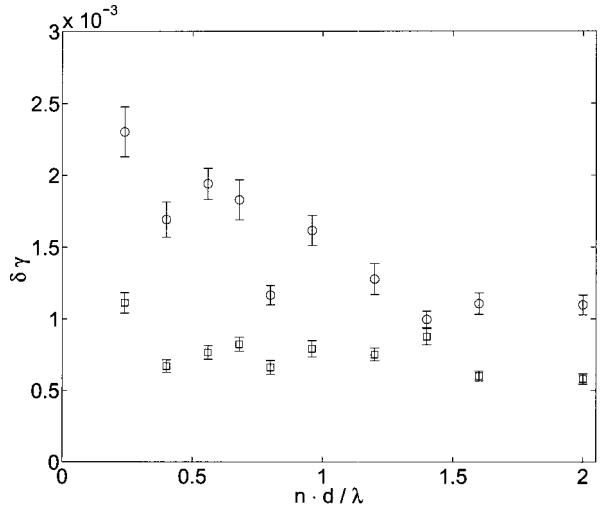

Fig. 9. Calculated standard deviation of lasing threshold $\delta\gamma$ as a function of dimensionless particle size. Squares and circles, TM and TE polarization, respectively.

To answer the above question we plotted the scattering efficiency, $Q_{sc} = \sigma_{sc}/\sigma_g$ (not to be confused with cavity Q), for a single cylinder (Fig. 8, inset): Thin and thick curves represent TE and TM polarization, respectively. One can see the significant difference in the characteristic particle size when the value of Q_{sc} increases above 1. This is the size, in fact, at which the weak Rayleigh scattering fails and one has to account for the interactions between particles. For TM modes the increase in the lasing threshold (as well as in l_t) should occur at $nd/\lambda \simeq 0.2$. Incidentally, this is the smallest value that we could reach numerically without jeopardizing numerical accuracy. So the answer to the question posed above is that we simply did not reach the transition that should occur at yet a smaller particle size. This difference in transition size for TE and TM modes has a simple physical explanation. For thin dielectric cylinders, as in three dimensions, scattering is dominated by dipolar scattering, for which analytical results are available[18]:

$$Q_{TM} = \frac{\pi^2}{8} x^3 (n^2 - 1)^2,$$

$$Q_{TE} = \frac{\pi^2}{4} x^3 \left(\frac{n^2 - 1}{n^2 + 1}\right)^2, \qquad \frac{Q_{TM}}{Q_{TE}} = \frac{(n^2 + 1)^2}{2}. \tag{6}$$

One can see that the difference in scattering strengths ratio is ~17 and reflects the stronger polarizability of a thin cylinder in the direction along the axis compared with the polarizability in the direction perpendicular to the axis. This numerical prefactor leads to the difference in characteristic size for two polarizations. Moreover, in the saturated regime the value of the average lasing threshold is relatively lower for TM than that for TE waves. This can be explained by stronger interference effects in TM polarization, which are equivalent to a scalar wave. In this respect the interference is harder to achieve for TE modes and leads to a higher threshold, as one can see from Fig. 8.

The difference between TE and TM lasing thresholds also is manifested in fluctuations (Fig. 9). Computational time has limited the number of disorder realizations and led to the relatively large error bars. Nevertheless, one can still conclude that there is a general trend to increasing fluctuations $\delta\gamma$ on decrease of the particle size, as was shown in the experiment. This increase occurs at different sizes for TE and TM polarizations, in line with the discussion above. Fluctuation for a TE field is generally higher than that for a TM field (Fig. 9). As mentioned above, the availability of two electric field polarizations in the former case is the cause of this difference.

We should also mention that one needs to exercise caution in comparing the results of 2D simulations with 3D experiments. Indeed, the dependence of the lasing threshold and of its fluctuation on the particle size is a dimension-dependent effect. As it can be seen from Table 1 and Fig. 9, $\delta\gamma$ showed similar trends in the 2D simulations and the 3D experiments. However, the normalized standard deviation $\delta\gamma/\langle\gamma\rangle$ behavior is different: in two dimensions it increased with decreasing d (Table 1), whereas in two dimensions it decreased for TE polarization (not shown). Further simulations performed on 3D random systems are necessary to resolve this discrepancy.

4. CONCLUSIONS

We prepared samples of monodisperse ZnO spheres of different sizes. Measurements of the lasing thresholds in these samples showed a drastic decrease in the value of the average lasing threshold from $d = 85$ nm to $d = 137$ nm. We attribute this phenomenon to the reduction of the random laser's cavity size. That size is believed to be related to transport mean free path l_t.[16] The rapid decrease of l_t was obtained in theoretical calculations as well as inferred from experimental measurements of the coherent backscattering cone. However, when the particle size increased from 137 to 617 nm the lasing threshold remained nearly constant; so did the transport mean free path. This behavior was interpreted in terms of dependent scattering, and it contradicts the expectation based on a low-density approximation.

We have also reported, for the first time to our knowledge, measurements of the fluctuation of the lasing threshold. In our samples the standard deviation of the lasing threshold decreased with increasing ZnO particle size. This decrease was also caused by a reduction of the random laser's cavity size. Inasmuch as the excitation area was kept constant, a small cavity size resulted in a large number cavities excited by a pump pulse. Improved averaging within the excitation spot led to smaller fluctuation of the laser threshold. This behavior was also observed in our finite-difference time-domain simulations of 2D random media.

ACKNOWLEDGMENTS

This research is supported partially by the National Science Foundation under grant DMR-0093949 and by the National Science Foundation Materials Research Science and Engineering Centers program (DMR-0076097) at the

Materials Research Center of Northwestern University. H. Cao acknowledges support from the David and Lucile Packard Foundation.

Corresponding author H. Cao may be reached by e-mail to h-cao@northwestern.edu.

REFERENCES

1. V. S. Letokhov, "Quantum statistics of multi-mode radiation from an ensemble of atoms," Sov. Phys. JETP **26**, 835–840 (1968).
2. H. Cao, "Lasing in disordered media," in *Progress in Optics*, E. Wolf, ed. (North-Holland, Amsterdam, 2003), Vol. 45, and references therein.
3. A. A. Chabanov and A. Z. Genack, "Photon localization in resonant media," Phys. Rev. Lett. **87**, 153901 (2001).
4. V. M. Apalkov, M. E. Raikh, and B. Shapiro, "Random resonators and prelocalized modes in disordered dielectric films," Phys. Rev. Lett. **89**, 016802 (2002).
5. A. Lagendijk and B. A. van Tiggelen, "Resonant multiple scattering of light," Phys. Rep. **270**, 143–215 (1996).
6. P. Sheng, *Introduction to Wave Scattering, Localization, and Mesoscopic Phenomena* (Academic, New York, 1995).
7. M. P. van Albada and A. Lagendijk, "Observation of weak localization of light in a random medium," Phys. Rev. Lett. **55**, 2692–2695 (1985).
8. P. E. Wolf and G. Maret, "Weak localization and coherent backscattering of photons in disordered media," Phys. Rev. Lett. **55**, 2696–2699 (1985).
9. Y.-L. Xu, "Electromagnetic scattering by an aggregate of spheres: far field," Appl. Opt. **36**, 9496–9508 (1997); computer codes are available at http://www.astro.ufl.edu/~xu/.
10. M. Patra, "Theory for photon statistics of random lasers," Phys. Rev. A **65**, 043809 (2002).
11. A. Taflove, *Computational Electrodynamics: The Finite Difference Time Domain Method* (Artech House, Boston, Mass., 1995).
12. X. Y. Jiang and C. M. Soukoulis, "Time dependent theory for random lasers," Phys. Rev. Lett. **85**, 70–73 (2000).
13. C. Vanneste and P. Sebbah, "Selective excitation of localized modes in active random media," Phys. Rev. Lett. **87**, 183903 (2001).
14. E. W. Seelig, R. P. H. Chang, A. Yamilov, and H. Cao, "Self-assembled 3D photonic crystals from ZnO colloidal spheres," Mater. Chem. Phys. **80**, 257–263 (2003).
15. Y. Ling, H. Cao, A. L. Burin, M. A. Ratner, X. Liu, and R. P. H. Chang, "Investigation of random lasers with resonant feedback," Phys. Rev. A **64**, 063808 (2001).
16. H. Cao, Y. Ling, J. Y. Xu, and A. L. Burin, "Probing localized states with spectrally resolved speckle techniques," Phys. Rev. E **66**, 025601 (2002).
17. J. X. Zhu, D. J. Pine, and D. A. Weitz, "Internal reflection of diffusive light in random media," Phys. Rev. A **44**, 3948–3959 (1991).
18. H. C. van de Hulst, *Light Scattering by Small Particles* (Dover, New York, 1981).
19. S. Kawato, T. Hattori, T. Takemori, and H. Nakatsuka, "Short-range interference effect in the diffusion of light in random media," Phys. Rev. B **58**, 6180–6193 (1998).
20. C. M. Soukoulis, M. Datta, and E. N. Economou, "Propagation of classical waves in random media," Phys. Rev. B **49**, 3800–3810 (1994).
21. X. Jing, P. Sheng, and M. Zhou, "Acoustic and electromagnetic quasimodes in dispersed random media," Phys. Rev. B **46**, 6513–6534 (1992).
22. D. Livdan and A. A. Lisyansky, "Diffusion of classical waves in random media with microstructure resonances," J. Opt. Soc. Am. A **13**, 844–850 (1996).
23. K. Busch, C. M. Soukoulis, and E. N. Economou, "Transport and scattering mean free paths of classical waves," Phys. Rev. B **50**, 93–98 (1994).
24. K. Busch and C. M. Soukoulis, "Transport properties of random media: an energy-density CPA approach," Phys. Rev. B **54**, 893–899 (1996).
25. C. F. Bohren and D. R. Huffman, *Absorption and Scattering of Light by Small Particles* (Wiley, New York, 1983).
26. S. Chandrasekhar, *Radiative Transfer* (Dover, New York, 1960).
27. P. Sheng, ed., *Scattering and Localization of Classical Waves in Random Media*, Vol. 8 of World Scientific Series on Directions in Condensed Matter Physics (World Scientific, Singapore, 1990).
28. A. Yamilov and H. Cao, "A study of random laser modes in disordered photonic crystals," http://arxiv.org/PS_cache/cond-mat/pdf/0209/0209680.pdf.